Mesoscopic magnetism in dielectric photonic crystal meta materials: topology and inhomogeneous broadening

Niels Asger Mortensen
nam@mic.dtu.dk

MIC – Department of Micro and Nanotechnology, NanoDTU, Technical University of Denmark, Bldg. 345 east, DK-2800 Kongens Lyngby, Denmark

Sanshui Xiao

MIC – Department of Micro and Nanotechnology, NanoDTU, Technical University of Denmark, Bldg. 345 east, DK-2800 Kongens Lyngby, Denmark

Didier Felbacq

GES UMR-CNRS 5650, Université de Montpellier II, Bât. 21, CC074, Place E. Bataillon, 34095 Montpellier Cedex 05, France

We consider meta materials made from a two-dimensional dielectric rod-type photonic crystal. The magnetic response is studied within the recently developed homogenization theory and we in particular study the effects of topology and inhomogeneous broadening. While topology itself mainly affects the Mie resonance frequency we find that the dispersion in the topological radius $\mathscr{R}$ of the dielectric rods may lead to significant inhomogeneous broadening and suppression of the negative-μ phenomena for $\delta\mathscr{R}/\mathscr{R}_0 \gg \varepsilon''/\varepsilon'$, with $\varepsilon = \varepsilon' + i\varepsilon''$ being the relative dielectric function of the rods. [DOI: 10.2971/jeos.2006.06019]

1 Introduction

The development of meta materials has led to renewed interest in the original work by Veselago on negative refraction [1] and the field of meta materials is in rapid growth. For more details we refer to recent reviews [2]–[4] as well as to recent special issues [5, 6]. In this work we consider a photonic crystal composed of high-index dielectric rods arranged in a two-dimensional lattice, see Figure 1A. For temporal harmonic modes the **H** field is governed by [7, 8]

$$\nabla \times \frac{1}{\varepsilon(\boldsymbol{r})} \nabla \times \boldsymbol{H}(\boldsymbol{r}) = \mu(\boldsymbol{r})\frac{\omega^2}{c^2}\boldsymbol{H}(\boldsymbol{r}) \tag{1}$$

where ε is the relative dielectric permittivity, μ is the relative magnetic permeability, c is the speed of light in vacuum, and $\omega = ck$ is the angular frequency with $k = 2\pi/\lambda$ being the free-space wave vector. For Nature's own dielectric materials we locally have, almost by definition, that $\mu(\boldsymbol{r}) \equiv 1$ so that everywhere in space $\boldsymbol{B}(\boldsymbol{r}) = \mu(\boldsymbol{r})\boldsymbol{H}(\boldsymbol{r}) \equiv \boldsymbol{H}(\boldsymbol{r})$ [8]. However, for artificial composite dielectric structures in the meta material limit, where the free-space wavelength λ is much longer than the characteristic length scale (periodicity) d of the underlying (quasi) periodic structure, one may for the slowly varying homogenized fields (envelopes) have an effective permeability μ_{eff} which is constant in space and which at certain frequencies deviates remarkably from the microscopic permeability, i.e. $\mu_{\text{eff}} \neq \mu$ and in particular it may become negative. The same apparent paradox is also possible for the dielectric response. As an example Figure 2 shows a plane-wave simulation [9] of Eq. (1) for the structure in Figure 1A with $\varepsilon = 200$ and $\mu = 1$ for the rods and $\varepsilon = \mu = 1$ for the background air region. For these inverse photonic crystal structures, the band structure and the photonic band-gap formation can be understood in terms of Mie resonances [10, 11]. Clearly, the band

structure reveals a strong hybridization at the frequency corresponding to the first Mie resonance of the rods as indicated by the dashed line. It is this resonance behaviour which make the rods behave as artificial magnetic atoms with the possibility for a negative-μ response.

In this work we extract the effective permeability by applying the recently derived mesoscopic homogenization theory for p-polarized fields by Felbacq and Bouchitté [12]–[14]. We in detail study the effective permeability μ_{eff} and the effect of the topology of the rods as well as the influence of spatial disorder/randomness and dispersion in the rod topology, compare panels (B) and (C) in Figure 1. For rods with a more arbitrary cross section Ω we define a topological radius $\mathscr{R}$ by

$$\mathscr{R} = 2\mathscr{A}/\mathscr{P} \tag{2}$$

where $\mathscr{A}$ is the area of Ω and $\mathscr{P}$ is the perimeter of its surface $\partial\Omega$, see Figure 1B. It is easily verified that a circular cross section of radius R gives $\mathscr{R} = R$. More generally, the topological radius $\mathscr{R}$ captures the qualitative resonance behaviour of the effective permeability as we shall see in the following.

Our results for more arbitrary topologies rely on approximative results for the spectral problem of the Helmholtz equation as employed recently by one of us in the context of diffusion dynamics, fluid flow, and ion transport in microfluidic problems [15]–[17].

2 MULTI-SCALE EXPANSION THEORY

We consider the problem of p-polarized fields corresponding to a magnetic field aligned parallel to the rods, see Figure 1A.
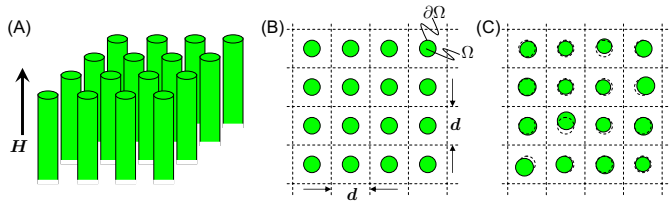

FIG. 1 (A) Photonic crystal consisting of parallel high-index dielectric rods. We consider the p-polarized case with the magnetic field parallel to the rods. (B) Top view of the photonic crystal with rods arranged in a periodic lattice with pitch d. (C) Top view of weakly disordered/random photonic crystal.

In the limit where $\lambda \gg d$ the problem posed by Maxwell's equations can be treated by a multi-scale expansion approach leading to an effective magnetic permeability given by [13]

$$\mu_{\text{eff}} = f \times \mu_{\text{air}} + (1-f) \times \mu_\Omega$$
$$= f + (1-f)\frac{\langle 1|m\rangle}{\langle 1|1\rangle} \qquad (3)$$

where $\mathscr{A} = \langle 1|1\rangle$ is the area of Ω, f is the air-filling fraction, and $|m\rangle$ is governed by

$$\nabla^2|m\rangle + k^2\varepsilon|m\rangle = 0, \quad \boldsymbol{r} \in \Omega \qquad (4a)$$
$$|m\rangle = 1, \quad \boldsymbol{r} \in \partial\Omega. \qquad (4b)$$

Above, we have used the Dirac *bra-ket* notation and inner products are defined as

$$\langle h|g\rangle = \int_\Omega d\boldsymbol{r}\, hg, \qquad (5)$$

where $h(\boldsymbol{r})$ and $g(\boldsymbol{r})$ are functions on Ω. Similarly, $|m\rangle$, or $m(\boldsymbol{r})$, in Eqs. (3) and (4) corresponds to the magnetic field component along the rods and $|1\rangle$ denotes the unity function.

In the following we assume a quadratic unit cell with area d^2, see Figure 1B, so that $f = 1 - \mathscr{A}/d^2$. As in Refs. [12]–[14] we solve the problem in a complete basis defined by the Helmholtz eigenvalue equation

$$\nabla^2|\psi_n\rangle + \kappa_n^2|\psi_n\rangle = 0, \quad \boldsymbol{r} \in \Omega, \qquad (6a)$$
$$|\psi_n\rangle = 0, \quad \boldsymbol{r} \in \partial\Omega, \qquad (6b)$$

with the basis functions being orthonormal, i.e. $\langle\psi_m|\psi_n\rangle = \delta_{nm}$. Obviously, the Ansatz

$$|m\rangle = |1\rangle + \sum_n \alpha_n|\psi_n\rangle \qquad (7)$$

fulfills the boundary condition and the expansion coefficients are readily determined by standard *bra-ket* manipulations. In this way we arrive at the following general expression for the effective permeability [12]

$$\mu_{\text{eff}} = 1 + \sum_n \frac{-k^2\varepsilon}{k^2\varepsilon - \kappa_n^2}\frac{|\langle 1|\psi_n\rangle|^2}{d^2}. \qquad (8)$$

The strength of this result is obviously the connection of μ_{eff} to the spectrum and eigenstates of the Helmholtz equation which have been studied in great detail in various contexts of physics, including membrane dynamics, the acoustics of drums, the single-particle eigenstates of 2D quantum dots, not to forget quantized conductance of quantum wires. Finally, the results of course in turn provides the direct link between μ_{eff} and the Mie resonances.

3 APPROXIMATE PROPERTIES OF THE SPECTRAL PROBLEM

In the following we utilize approximate results for the spectral problem and its dependence on geometry. We start by introducing the effective area $\mathscr{A}_n = |\langle 1|\psi_n\rangle|^2$ so that Eq. (8) is rewritten as

$$\mu_{\text{eff}} = 1 + (1-f)\sum_n \frac{-k^2\varepsilon}{k^2\varepsilon - \kappa_n^2}\frac{\mathscr{A}_n}{\mathscr{A}}$$
$$\simeq 1 + (1-f)\frac{-k^2\varepsilon}{k^2\varepsilon - \kappa_1^2}\frac{\mathscr{A}_1}{\mathscr{A}} \qquad (9)$$

where we in the second line have truncated the rapidly converging sum making the approximation valid in the vicinity of the main resonance.

In Table 1 we have listed the first eigenvalue κ_1 and the corresponding effective area $\mathscr{A}_1$ for a number of different geometries.

	$(\kappa_1\mathscr{R})^2$	$\mathscr{A}_1/\mathscr{A}$
circle	$\chi_{00}^2 \simeq 5.78^a$	$4/\chi_{00}^2 \simeq 0.69^a$
quarter-circle	5.08^b	0.65^b
half-circle	5.52^b	0.64^b
ellipse(1:2)	6.00^b	0.67^b
ellipse(1:3)	6.16^b	0.62^b
ellipse(1:4)	6.28^b	0.58^b
triangle(1:1:1)	$4\pi^2/9 \simeq 4.39^c$	$6/\pi^2 \simeq 0.61^c$
triangle(1:1:$\sqrt{2}$)	$\frac{5\pi^2}{(2+\sqrt{2})^2} \simeq 4.23^a$	$512/9\pi^4 \simeq 0.58^a$
square(1:1)	$\pi^2/2 \simeq 4.93^a$	$64/\pi^4 \simeq 0.66^a$
rectangle(1:2)	$5\pi^2/9 \simeq 5.48^a$	$64/\pi^4 \simeq 0.66^a$
rectangle(1:3)	$5\pi^2/8 \simeq 6.17^a$	$64/\pi^4 \simeq 0.66^a$
rectangle(1:4)	$17\pi^2/25 \simeq 6.71^a$	$64/\pi^4 \simeq 0.66^a$
pentagon	5.20^b	0.67^b
hexagon	5.36^b	0.68^b

TABLE 1 Central dimensionless parameters for different geometries. [a] See e.g. [18] for the eigenmodes and eigenspectrum. [b] Data obtained by finite-element simulations. [c] See e.g. [19] for the eigenmodes and eigenspectrum.

For the numerical results we have employed a finite-element method with an adaptive mesh algorithm (Comsol multi-physics) ensuring fast convergence of both eigenvalues and eigenstates. Inspecting the column for the eigenvalue κ_1^2 in Table 1 we note that the numbers do not in general change much from geometry to geometry, despite the variation in topology. The small spread originates in the normalization by the topological radius $\mathscr{R}$, see Eq. (2). For the effective area $\mathscr{A}_1$ we likewise observe a modest variation. It is worthwhile

emphasizing the results for a circular cross section which become good approximations for also other relatively compact topologies. In the following we thus use the approximation that $\kappa_1 \sim \chi_{00}/\mathscr{R}$ and $\mathscr{A}_1/\mathscr{A} \sim 4/\chi_{00}^2$ where $\chi_{00} \simeq 2.405$ is the first zero of the Bessel function, i.e. $J_0(\chi_{00}) = 0$. With these approximations we finally arrive at

$$\mu_{\text{eff}} \simeq 1 + (1-f)\frac{4}{\chi_{00}^2}\frac{-(k\mathscr{R})^2\varepsilon}{(k\mathscr{R})^2\varepsilon - \chi_{00}^2}$$

$$= 1 + (1-f)\frac{4}{\chi_{00}^2}\frac{-\varepsilon}{\varepsilon - \left(\frac{\chi_{00}}{2\pi}\right)^2\left(\frac{\lambda}{\mathscr{R}}\right)^2} \quad (10)$$

where all the dependence on geometry is captured by the topological radius $\mathscr{R}$.

We may now estimate the resonance wavelength. Suppose that $\varepsilon = \varepsilon' + i\varepsilon''$, then for weakly absorbing materials, $\varepsilon'' \ll \varepsilon'$, we have the resonance around

$$\lambda^* \simeq \frac{2\pi}{\kappa_1}\sqrt{\varepsilon'} \approx \frac{2\pi}{\chi_{00}}\sqrt{\varepsilon'}\,\mathscr{R} \quad (11)$$

with a line width of the order

$$\delta\lambda \sim \frac{2\pi}{\chi_{00}}\frac{\varepsilon''}{\sqrt{\varepsilon'}}\mathscr{R}. \quad (12)$$

As expected the line width reflects the damping due to ε'' in the high-index material. Furthermore, we may also estimate the magnitude of the effective magnetic response. Just below the resonance the real part is bounded by

$$\text{Re}\{\mu_{\text{eff}}\} \gtrsim 1 - \frac{2}{\chi_{00}^2}(1-f)\frac{\varepsilon'}{\varepsilon''} \quad (13)$$

while for the imaginary part

$$\text{Im}\{\mu_{\text{eff}}\} \lesssim \frac{4}{\chi_{00}^2}(1-f)\frac{\varepsilon'}{\varepsilon''}. \quad (14)$$

The above results illustrate how ε, f, and $\mathscr{R}$ influence the magnetic response. Obviously, a negative permeability requires that $\varepsilon' \gg \varepsilon''$. On the other hand, some absorption is of course needed to have a finite line width instead of a delta-function-like response which would suffer tremendously from the inevitable effects of inhomogeneous broadening. We shall return to this in Section 5.

4 COMPARISON TO NUMERICAL RESULTS

The validity of the assumptions underlying Eq. (3) has been tested in Refs. [12]–[14] by comparing simulated transmission spectra of the real photonic crystal to spectra based on the corresponding homogenized meta material. In this work we thus assume Eq. (3) valid and focus on checking the quality of the approximate result in Eq. (10). We do this by comparing the outcome of Eq. (10) to numerical solutions of the original problem posed by Eq. (3). We use a finite-element method with an adaptive mesh algorithm (Comsol multiphysics) for this purpose. For the dielectric function we use $\varepsilon = 200 + 5i$ as in Refs. [12]–[14]. Figure 2 illustrates the corresponding photonic band structure.
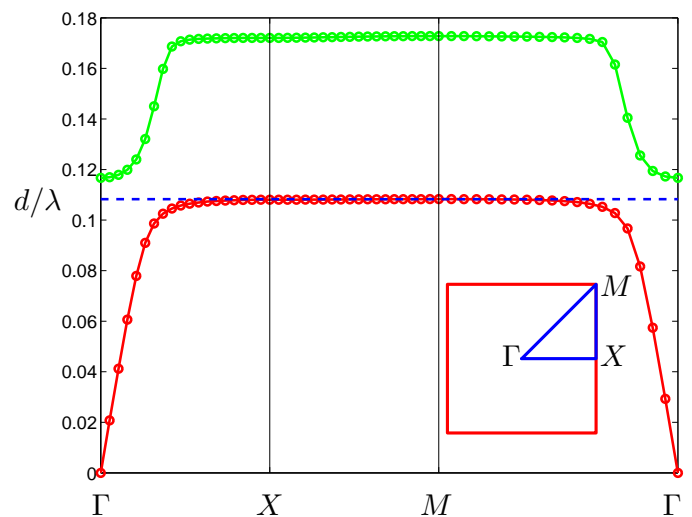

FIG. 2 Plane-wave simulations of photonic band structure for a $d \times d$ square lattice of rods of circular cross section with $\varepsilon = 200$, see Figure 1B. The air-filling fraction $f \simeq 80.37\%$ corresponding to a rod of radius $R = \mathscr{R} = d/4$. The dashed line shows the fundamental Mie resonance of an isolated dielectric rod, Eq. (11).

Clearly, there is a strong hybridization at the frequency corresponding to the isolated Mie resonance of the rod, see Eq. (11). It is this avoided crossing which causes strong resonance in the effective permeability that is observed in Figure 3.
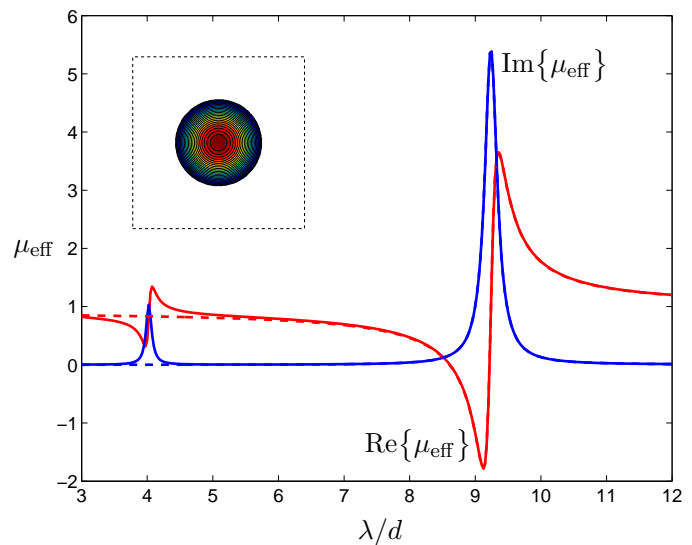

FIG. 3 Effective permeability μ_{eff} versus normalized wavelength λ/d for a rod with $\varepsilon = 200 + 5i$ in a quadratic $d \times d$ unit cell with an air-filling fraction $f \simeq 80.37\%$ corresponding to a rod of radius $R = \mathscr{R} = d/4$. The inset illustrates the unit cell as well as the function m at a wavelength above resonance. The solid lines are numerical exact solutions based on a finite-element (adaptive mesh) solution of Eq. (4) while the dashed lines show the approximate result in Eq. (10).

The approximate result in Eq. (10) works excellently near the main resonance for rods with circular cross section as seen in Figure 3 while the approximation of course doesn't capture high-order modes due to the truncation of the summation in Eq. (9). In the following we go a step further and test the result for highly non-circular geometries. Figure 4 illustrates results for one such example.
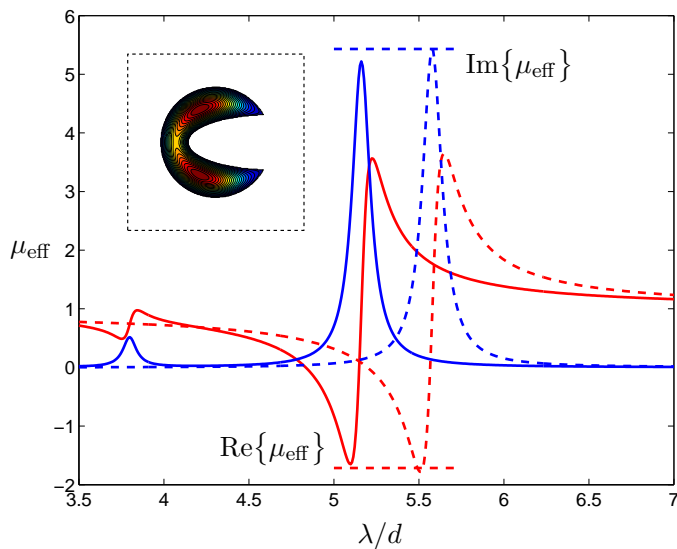
FIG. 4 Effective permeability μ_{eff} versus normalized wavelength λ/d for a rod with $\varepsilon = 200 + 5i$ in a quadratic $d \times d$ unit cell with an air-filling fraction $f \simeq 80.37\%$. The inset illustrates the unit cell as well as the function m at a wavelength above resonance. The highly non-circular cross section has a topological radius of $\mathscr{R} \simeq 0.151 \times d$. The solid lines are numerical exact solutions based on a finite-element (adaptive mesh) solution of Eq. (4) while the dashed lines show the approximate result in Eq. (10). The horizontal dashed lines show the limits in Eqs. (13) and (14).

As seen there is a good qualitative agreement and since the geometry is highly non-circular, see inset, the quantitative agreement is perhaps better than expected. Note how the change in topological radius $\mathscr{R}$ scales the resonance wavelength λ^* and the line width $\delta\lambda$ compared to the circular case, Figure 3, in accordance with Eq. (11) while the conservation of the air-filling fraction f leads to the same magnitude of the response in accordance with Eqs. (13) and (14) which depend only on f, but not on $\mathscr{R}$.

5 INHOMOGENEOUS BROADENING

The present results suggest that shape plays only a minor role and mainly affects the particular value of the resonance frequency (which is proportional to the topological radius $\mathscr{R}$) while the air-filling fraction f and the dielectric function $\varepsilon = \varepsilon' + i\varepsilon''$ tend to govern the magnitude of the effective magnetic response. This suggests that homogenized materials will not be strongly influenced by spatial disorder/randomness conserving the average air-filling fraction while shape dispersion (dispersion in the topological radius, possibly also influencing the average air-filling fraction) will give rise to a smearing of the resonance phenomena. Suppose that for a particular topological radius $\mathscr{R}_0$ the resonance wavelength is $\lambda_0^* = \alpha\mathscr{R}_0$, see Eq. (11), and that the width of the resonance is $\delta\lambda_0$. Assuming a Gaussian distribution of $\mathscr{R}$,

$$P(\mathscr{R}) \propto \exp\left[-\left(\frac{\mathscr{R} - \mathscr{R}_0}{\delta\mathscr{R}}\right)^2\right], \qquad (15)$$

and neglecting the dependence of the intrinsic line width $\delta\lambda_0$ on $\mathscr{R}$ we get an inhomogeneous suppression of the resonance

magnitude by a factor Π,

$$\Pi = \frac{1}{\sqrt{1 + \alpha^2 \left(\frac{\delta\mathscr{R}}{\delta\lambda_0}\right)^2}}, \qquad (16)$$

and an inhomogeneous broadening of the resonance by a factor Π^{-1},

$$\delta\lambda \sim \Pi^{-1}\delta\lambda_0. \qquad (17)$$

Thus, inhomogeneous broadening will be negligible if $\alpha\left(\frac{\delta\mathscr{R}}{\delta\lambda_0}\right) \ll 1$ corresponding to

$$\frac{\delta\mathscr{R}}{\mathscr{R}_0} \ll \frac{\varepsilon''}{\varepsilon'}. \qquad (18)$$

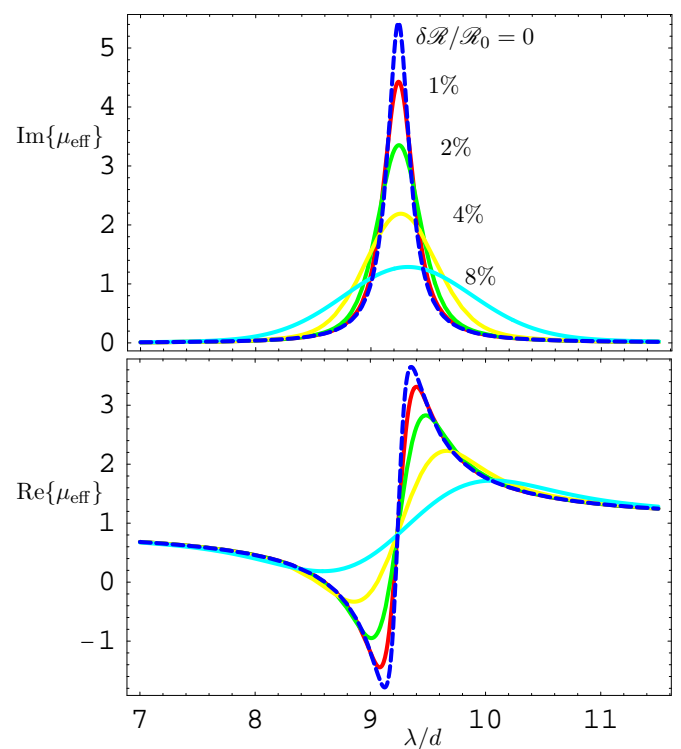Figure 5 illustrates these results in the case of rods of circular cross section as in Figure 3.

FIG. 5 Inhomogeneous broadening of the effective permeability μ_{eff} for rods with a circular cross section in a quadratic $d \times d$ unit cell with an average air-filling fraction $f_0 \simeq 80.37\%$ corresponding to rods with an average radius $R_0 = \mathscr{R}_0 = d/4$. The dashed curves show the intrinsic line width corresponding to the results in Figure 3.

The results are obtained from a numerical evaluation of $\int_0^\infty d\mathscr{R} \, \mu_{\text{eff}}(\mathscr{R}) P(\mathscr{R})$ with μ_{eff} given by Eq. (10). As also suggest by Eq. (18) a size dispersion with a relative variation comparable to $\varepsilon''/\varepsilon'$ preserves the negative-μ phenomena while larger variations will result in a positive μ_{eff}.

6 CONCLUSION

We have studied the magnetic response of rod-type dielectric meta materials within the recently developed homogenization theory [12] and we have in particular investigated the effects of topology and inhomogeneous broadening. We predict that topology itself mainly affects the Mie resonance frequency

while the resonance shape mainly depends on the air-filling fraction and the ratio $\varepsilon'/\varepsilon''$ with $\varepsilon = \varepsilon' + i\varepsilon''$ being the relative dielectric function of the rods. Furthermore, we argue that randomness/disorder conserving the air-filling fraction will have a limited influence on the negative-μ phenomena while dispersion in the topological radius $\mathscr{R}$ of the rods may lead to significant inhomogeneous broadening and suppression of the phenomena.

ACKNOWLEDGMENTS

References

[1] V. G. Veselago, "Electrodynamics of substances with simulataneously negative values of ε and μ." Sov. Phys. Uspekhi-USSR **10**, 509 (1968).

[2] J. B. Pendry and D. R. Smith, "Reversing light with negative refraction" Physics Today **57**, (6) 37 – 43 (2004).

[3] D. R. Smith, J. B. Pendry, and M. C. K. Wiltshire, "Metamaterials and negative refractive index" Science **305**, 788 – 792 (2004).

[4] C. M. Soukoulis, "Bending Back Light – The Science of Negative Index Materials" Optics & Photonics News **17**, (6) 16 – 21 (2006).

[5] J. B. Pendry, "Focus issue: Negative refraction and metamaterials - Introduction" Opt. Express **11**, 639 – 639 (2003).

[6] A. Lakhtakia and M. McCall, "Focus on Negative Refraction" New J. Phys. **7**, doi:10.1088/1367-2630/7/1/E03 (2005).

[7] J. D. Jackson, *Classical Electrodynamics* (John Wiley & Sons, New York, 1962).

[8] J. D. Joannopoulos, R. D. Meade, and J. N. Winn, *Photonic crystals: molding the flow of light* (Princeton University Press, Princeton, 1995).

[9] S. G. Johnson and J. D. Joannopoulos, "Block-iterative frequency-domain methods for Maxwell's equations in a planewave basis" Opt. Express **8**, 173 – 190 (2001).

[10] M. M. Sigalas, C. M. Soukoulis, C. T. Chan, and D. Turner, "Localization of electromagnetic waves in two-dimensional disordered systems" Phys. Rev. B **53**, 8340 – 8348 (1996).

[11] E. Lidorikis, M. M. Sigalas, E. N. Economou, and C. M. Soukoulis, "Gap deformation and classical wave localization in disordered two-dimensional photonic-band-gap materials" Phys. Rev. B **61**, 13458 – 13464 (2000).

[12] D. Felbacq and G. Bouchitte, "Theory of mesoscopic magnetism in photonic crystals" Phys. Rev. Lett. **94**, 183902 (2005).

[13] D. Felbacq and G. Bouchitte, "Negative refraction in periodic and random photonic crystals" New J. Phys. **7**, 159 (2005).

[14] D. Felbacq and G. Bouchitte, "Left-handed media and homogenization of photonic crystals" Opt. Lett. **30**, 1189 – 1191 (2005).

[15] N. A. Mortensen and H. Bruus, "Universal dynamics in the onset of a Hagen-Poiseuille flow" Phys. Rev. E **74**, 017301 (2006).

[16] N. A. Mortensen, L. H. Olesen, and H. Bruus, "Transport coefficients for electrolytes in arbitrarily shaped nano- and microfluidic channels" New J. Phys. **8**, 37 (2006).

[17] N. A. Mortensen, F. Okkels, and H. Bruus, "Universality in edge-source diffusion dynamics" Phys. Rev. E **73**, 012101 (2006).

[18] P. M. Morse and H. Feshbach, *Methods of Theoretical Physics* (McGraw–Hill, New York, 1953).

[19] M. Brack and R. K. Bhaduri, *Semiclassical Physics* (Addison Wesley, New York, 1997).